

Tailoring of Single-Crystalline Complex Ta₅Si₃ Nanostructures: From Networked Nanowires to Nanosheets

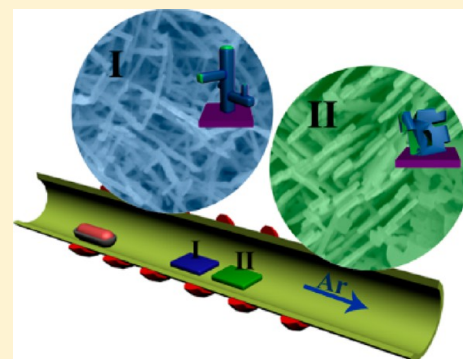
Mohammad Norouzi Banis,[†] Yong Zhang,[†] Qiangfeng Xiao,[‡] Mei Cai,[‡] Ruying Li,[†] and Xueliang Sun^{*†}

[†]Department of Mechanical and Materials Engineering, The University of Western Ontario, London, Ontario N6A 5B9 Canada

[‡]General Motors R&D Center, Warren, Michigan 48090-9055, United States

Supporting Information

ABSTRACT: Single-crystalline Ta₅Si₃ nanostructures with a complex morphology were synthesized through a catalyst-free, chemical vapor deposition method under low pressures. The morphology, structure, and composition of deposited nanostructures were studied by scanning electron microscopy, X-ray diffraction, and high-resolution transmission electron microscopy. These nanostructures have lengths of up to several tens of micrometers and an average thickness of 13 nm. It was found that the formation of networked Ta₅Si₃ nanostructures is highly sensitive to the vapor pressure of tantalum chloride and silica and is based on a vapor–solid mechanism. Results indicate that, with the decrease of silica vapor pressure, the Ta₅Si₃ networked nanowires evolve into networked nanoribbons and nanosheets via two-dimensional growth. Cyclic voltammetry measurements of the Ta₅Si₃ nanostructures show superior electrochemical capacitance properties of nanosheets compared to nanowires. It is expected that these nanostructures have great potential applications for nanodevices in electronic and energy related applications.



1. INTRODUCTION

As a family of intermetallic compounds between metals and silicon, metal silicides have attracted great interest owing to their excellent electrical properties,^{1–6} superior thermal stability^{5–7} and oxidation resistance.⁶ These materials constitute an important group of compounds that are used in modern silicon-based microelectronics^{1–3,6,8,9} and optoelectronic devices.^{10,11} Metal silicides have been used as Ohmic contacts,^{2,3,12} interconnects^{3,12} and gate materials for CMOS microelectronic transistors,^{3,13,14} or stable, inexpensive thermoelectric materials.^{2,15} Rapid progress in microelectronics and miniaturization of electronic devices requires the dimensional shrinkage of its components, including metal silicides.^{3,4,9,13,16} For this purpose, extensive research has been focused on the synthesis of single-crystalline one-dimensional metal silicide nanostructures, such as Ti₅Si₃,⁴ TiSi₂,¹⁷ FeSi₂,¹⁸ NiSi₂,¹⁹ and TaSi₂.^{3,5,12} However, because of their high melting point and susceptibility to silicon or metal oxide formation, the controlled synthesis of metal silicide nanostructures is challenging. Various methods based on the vapor deposition process, such as silydation of metal nanowires or use of metal halides and chlorides, have been developed.²

Recently, tantalum silicide nanostructures such as TaSi₂ nanowires have been synthesized by annealing FeSi₂ and NiSi₂ thin films on a silicon substrate in an ambient containing Ta vapor.^{3,5,12} TaSi₂ is a promising material as field emitters in field emission applications and interconnections between individual nanodevices due to their metallic characteristics and high thermal stability.^{5,12} Ta₅Si₃ thin films have also been

studied for high-temperature applications and as thermoelectric materials.^{7,15}

Here, we report a facile method for the synthesis of tantalum silicide networked nanostructures by low-pressure chemical vapor deposition method (LPCVD). The nanostructures are deposited on a conductive and porous substrate (carbon microfibers) for electrochemical applications similar to previous reports on the synthesis of W₁₈O₄₉,²⁰ SnO₂,²¹ and Ti₅Si₃.⁴ The growth mechanism of unique nanostructures of tantalum silicides, based on the formation of silicon oxide passive layer, is discussed in detail. We found that the overall shape and crystal structure of the products is sensitive to the composition of the carrier gas and partial pressure of silica on the surface of the substrate.

2. EXPERIMENTAL METHODS

Ta₅Si₃ nanostructures were synthesized via a home-built LPCVD system. TaCl₅ (Aldrich, 99.9%) and Si (Aldrich, 99%) powder were used as the starting materials. The commercially available carbon paper obtained from E-TEK, a division of De Nora North America, Somerset, NJ, composed of carbon microfibers of 5–10 μm in diameter was used as substrates. The substrates were placed on an alumina boat covering the silicon powder. The source material and the substrates were inserted into a quartz tube, and it was mounted on a horizontal electric furnace. TaCl₅ powder was positioned upstream in the CVD chamber (200 °C), and Si powder was placed in the high-temperature region (900 °C). To purge the oxygen from the system,

Received: April 13, 2013

Revised: November 24, 2013

Published: December 9, 2013

the pressure of the CVD chamber was decreased to 1 mbar before argon was flushed into the system and the pressure was increased to over 50 mbar. This process was repeated three times. The system was then heated to a set temperature with a heating rate of $10\text{ }^{\circ}\text{C min}^{-1}$ and kept at this temperature for 1 h. During the experiment, the pressure inside the chamber was maintained at 5 mbar with a continuous flow of Ar (purity, 99.999%), which also acted as the carrier gas. After cooling down to room temperature, a dark layer was observed deposited on the substrate.

The morphology of the products was examined under a field emission scanning electron microscope (SEM, Hitachi S4800) operated at 5.0 kV equipped with an energy-dispersive X-ray analysis (EDX), and a transmission electron microscope operated at an accelerating voltage of 100 kV (TEM, Hitachi 7000). Further detailed morphology characterization was carried out by a high-resolution transmission electron microscope (HRTEM, JEOL 2010) and selected area electron diffraction (SAED) operated at 200 kV. The crystal structure of the products was characterized by an X-ray diffractometer using $\text{Co K}\alpha$ ($\lambda = 0.179\text{ nm}$) radiation operated at 30 kV and 15 mA (XRD, Bruker D8). Using an Autolab potentiostat/galvanostat (model PGSTAT-30), the electrochemical behavior of the samples directly deposited on carbon paper was evaluated by cyclic voltammetry in 0.5 M H_2SO_4 saturated with N_2 at room temperature and scanned from -658 to 542 mV versus a saturated Hg/HgSO_4 (K_2SO_4) reference electrode at a scanning rate of 50 mV/s .

3. RESULTS AND DISCUSSION

Figure 1a,b shows a high density of as-grown products synthesized along the CVD chamber. The reaction area can

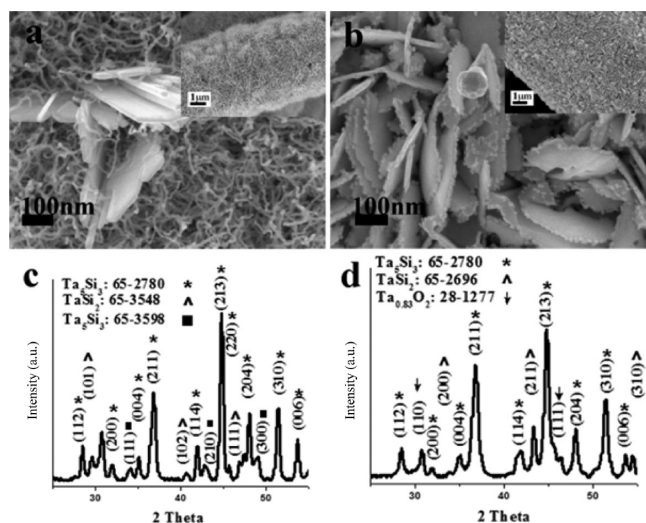


Figure 1. SEM images and XRD pattern of nanostructures deposited along the CVD chamber: (a, c) initial section (NNWs) and (b, d) end section (NNRs and NSs) of the reaction area.

be divided into two regions, with networked nanowires (NNWs, Figure 1a) in the initial region (upstream) and networked nanoribbons and nanosheets (NNRs and NSs, Figure 1b) in the end region (downstream).

SEM observations indicate (Figure 1a) that NNWs have lengths of up to tens of micrometers. The major diffraction peaks from the XRD pattern of these nanostructures shown in Figure 1c is ascribed to the tetragonal Ta_5Si_3 phase (JCPDS 65-2780), which is the most stable form of Ta_5Si_3 at room temperature ($D8_1$). The remaining peaks were assigned to Ta_5Si_3 (JCPDS 65-3598) and TaSi_2 (JCPDS 65-3548).

SEM images (Figure 1b) of NNRs deposited on the substrate show comparable dimensions to NNWs, with lengths of up to

tens of micrometers and an average thickness of 15 nm. These nanostructures have well-defined shapes with sharp edges, indicating a well-crystallized structure. Detailed SEM observations reveal the presence of branched NNWs and small imperfections and gaps in the NSs. These features can be an indication of two-dimensional growth of nanostructures along certain crystal directions. According to the XRD patterns (Figure 1d) of these nanostructures, similar to NNWs, the major phase in this reaction region is the tetragonal Ta_5Si_3 phase (JCPDS 65-2780). However, XRD patterns indicate that the minor phases are composed of TaSi_2 (JCPDS 65-2696) and $\text{Ta}_{0.83}\text{O}_2$ (JCPDS 28-1277). The increase in the concentration of oxygen along the CVD chamber and the presence of tantalum oxide are confirmed by the EDX results.

TEM and HRTEM analysis further reveals the unique crystal structures of as-deposited nanomaterials. TEM images (Figure 2a) of NNWs clearly illustrate the branching of these

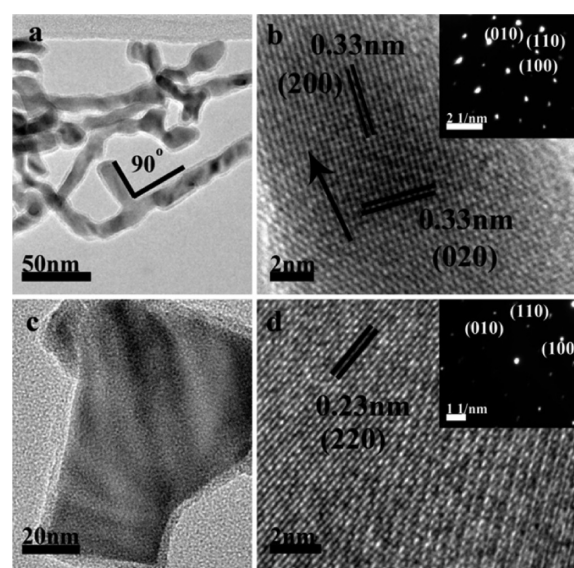


Figure 2. TEM and HRTEM images of (a, b) NNWs and (c, d) NNRs and NSs.

nanostructures. As shown in Figure 2a, the branches exist in planes perpendicular to the nanowires, which is consistent with the tetragonal symmetry ($D8_1$) of Ta_5Si_3 . Furthermore, TEM images reveal that these nanostructures have a core shell structure with an average inner diameter of 13 nm and a shell thickness of 2 nm. Figure 2b, a HRTEM image of the core section of a NNW, clearly shows lattice fringes, confirming the single-crystalline nature of the NNWs. The selected area electron diffraction (SAED) pattern obtained from the NNWs (inset Figure 2b) shows a regular spot pattern, which can be fully indexed to the tetragonal ($D8_1$) Ta_5Si_3 crystal structure (JCPDS 65-2780). This pattern is in a good agreement with the XRD results shown in Figure 1c. The lattice spacing of 0.33 nm measured in Figure 2b corresponds well to $\{200\}$ planes of the Ta_5Si_3 phase identified in the SAED pattern, indicating $\langle 010 \rangle$ to be the growth direction of the NNWs. The lack of lattice fringes in the HRTEM observation of the shell section covering the Ta_5Si_3 nanostructures and the well-ordered SAED pattern reveal the amorphous nature of the shell. EDX analysis of these nanostructures demonstrates the presence of oxygen on the nanostructures, which leads to the assumption of SiO_x layer formation on the Ta_5Si_3 nanostructures.

Figure 2c is the TEM image of NNRs and NSs, showing 90° edges. This suggests a two-dimensional growth of these nanostructures similar to NNWs. Furthermore, as seen in NNWs, an amorphous SiO_x layer with an average thickness of 2 nm covers the NNRs. The lattice fringes clearly shown in the HRTEM image of these nanostructures (Figure 2d) imply these nanostructures to be single-crystalline, and the respective SAED pattern (inset of Figure 2d) corresponds to the tetragonal Ta₅Si₃ crystal structure (JCPDS 65-2780). The lattice spacing of 0.22 nm shown in Figure 2d can be matched to the {220} plane of this crystal structure.

3.1. Time-Dependent Growth of Nanostructures. To better understand the morphological evolution and formation of networked nanoribbons, and demonstrate the relationship between the growth of these nanostructures and network nanowires, a time-dependent growth study was carried out at the downstream reaction area. Figure 3 shows the morpho-

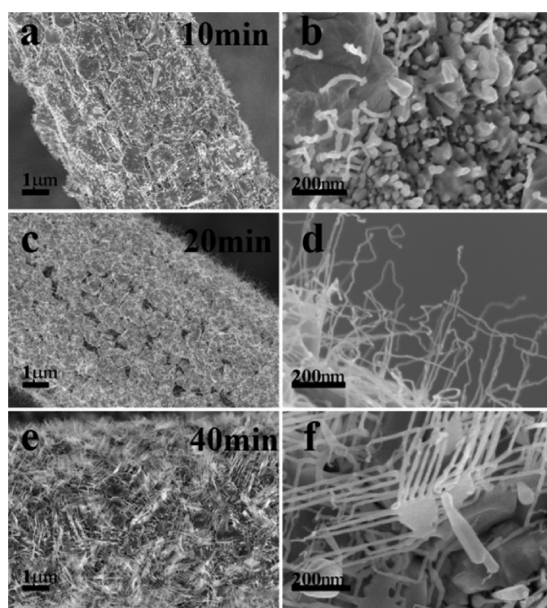


Figure 3. Evolution of Ta₅Si₃ nanostructures deposited on carbon microfibers in the end section of the reaction area by the increase of experiment time: (a, b) 10 min, (c, d) 20 min, (e, f) 40 min.

logical evolution of nanostructures deposited on the substrates in the NNR and NSs growth region versus time. As shown in Figure 3a, a thin layer composed of nanoparticles and microparticles is deposited on the substrate during the initial stages of the growth process. At this stage these nanoparticles and edges of microparticles act as nucleation sites for the growth of small nanorods. On the basis of the XRD results (Figure 1: the presence of TaSi₂ and Ta₅Si₃ patterns) and HRTEM (Figure 2) observations of the Ta₅Si₃ nanostructures, it can be concluded that these nanoparticles have TaSi₂ and Ta₅Si₃ crystal structures. Similar to previous reports on the synthesis of TiSi₂^{17,22} and MnO²⁶ nanostructures, these intermediate layers formed on the substrate can facilitate the deposition and growth of Ta₅Si₃ nanostructures.

By increasing the growth time, the nanorods grow into networked nanostructures. Further increase of synthesis time results in the development of the networked nanorods to nanoribbons and nanosheets, with nanoribbons and nanowires extending from their tips, indicating a two-dimensional growth with different growth rates. In addition, these observations

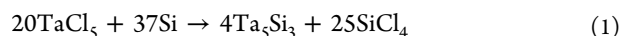
clarify the presence of imperfections between the NNRs and the NSs.

3.2. Growth Mechanism. **3.2.1. Ta₅Si₃ Formation.** On the basis of the above results, a growth mechanism can be proposed for the synthesis of Ta₅Si₃ nanostructures. Independent from the synthesis method in vapor-based processes, two main growth mechanisms have been proposed for the synthesis of metal-containing nanostructures. Catalyst-assisted growth of nanostructures or the vapor–liquid–solid mechanism (VLS) has been proposed for the growth of many metal-based nanostructures.^{4,22} This mechanism mainly features the presence of solidified droplets at the tip of synthesized nanostructures. The lack of catalyst nanoparticles and the absence of these droplets at the tip of Ta₅Si₃ nanostructures imply a non-VLS growth mechanism. The main catalyst-free growth of nanostructures is the vapor–solid mechanism (VS), in which the synthesis of nanostructures is influenced primarily by the crystal properties of nanostructures deposited, the substrates, and chemical species in the synthesis chamber.

In this study, similar to previous reports on the synthesis of metal silicides, a VS growth mechanism can be employed to explain the growth of Ta₅Si₃ nanostructures. However, in contrast to previous reports, the silicide nanostructures are deposited on a non-silicon substrate and experimental results show that the morphology of the nanostructures is sensitive to growth parameters.

Several studies have reported the formation of Ta₅Si₃ via the reaction between TaCl₅ and silicon species such as SiH₄ for synthesis of thin films.^{23,24} Williams et al.²³ studied the deposition of Ta₅Si₃ and TaSi₂ via reaction of TaCl₅ with different silicon sources, such as solid silicon and SiH₄. They proposed several possible reactions between the precursors and concluded that the crystal structure and stoichiometry of the final product is dependent on the ratio of tantalum and silicon reactive species.

According to the experimental observations in this study and previous reports on the synthesis of TaSi_x thin films, it is suggested that the deposition of tantalum silicides occurs via the following reaction



The formation of the SiO₂ layer observed around the nanostructures deposited on the substrates can occur via reaction between the silicon reactive species such as silicon chloride formed in reaction 1 and oxygen in the CVD chamber. The origin of oxygen is assumed to be from air leakage, residue oxygen in the chamber, and oxygen trapped in the system or source material.

3.2.2. Networked Nanostructure Formation. To explain the formation of various morphologies along the CVD chamber and propose a growth mechanism, a good understanding of the conditions in the CVD chamber is required. In this study, as observed under SEM, the morphology of Ta₅Si₃ nanostructures gradually evolves, implying a gradual change in the experimental conditions along the CVD chamber. Careful setup of the CVD system ensured a consistent temperature and gas flow in the experiment chamber. However, because of the nature of the CVD process and powder form of the source material, there is a concentration gradient of TaCl₅ vapor along the CVD chamber as it is consumed in the above reaction (evident from EDX results). This, consequently, decreases the concentration of silicon reactive species along the CVD chamber, decreasing the partial pressure of silicon, which

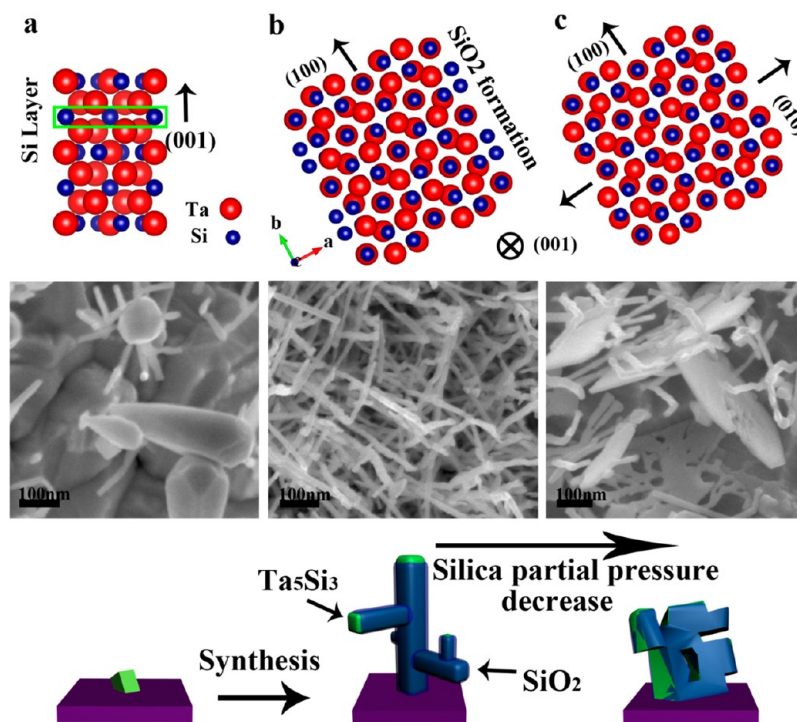


Figure 4. Schematic diagram of growth process of Ta_5Si_3 nanostructures with silica controlled morphologies: Ta_5Si_3 (a) nanocrystals, (b) NNWs, and (c) NRRs and NSs.

plays an important role in the formation of different types of Ta_5Si_3 nanostructures.

To date, there have been several reports of synthesis of metal, metal silicides, and metal oxide nanostructures, such as networked nanowires, nanoribbons, and nanosheets, via metal chlorides using the VS mechanism.^{2,4,25,27–29}

In these studies, two main processes have been proposed for the change from one-dimensional to two-dimensional growth and finally formation of networked nanostructures via the VS mechanism. The first process is based on non-equilibrium kinetic growth caused by supersaturation of reactive species such as oxygen and aluminum suboxides for the synthesis of aluminum oxide networked nanostructures, which may allow the formation of a low surface energy tip, favoring the 2D growth of the nanostructures.^{28,30} In our study, however, in contrast to these reports, the 2D nanostructures are synthesized in regions with lower concentration of reactive species and in higher surface energy directions.

The second growth mechanism is based on Zhang et al.'s^{27,29} result on controlled growth of nanosheets via SiO_2 vapor pressure. They proposed partial coverage of low surface energy planes of nanocrystals by a silica sheath. This sheath, induces a 2D growth of nanocrystals due to the positive feedback between the imbalance of silica coverage on different planes.

The growth process in the latter case closely corresponds to results observed in this study. Figure 4 shows a schematic diagram and corresponding SEM images indicating the growth mechanism of Ta_5Si_3 nanostructures. On the basis of this growth mechanism, in the initial stage of the synthesis process, Ta_5Si_3 nanocrystals are formed via reaction (1) (Figure 4a) on the intermediate layer covering the substrate. During the experiment, Ta and Si species are deposited on various crystal planes of these nanocrystals. According to the Ta_5Si_3 (D8_1) unit cell illustrated in Figure 4a, these crystal structures have Si-rich planes parallel to the (001) crystal plane. During the CVD

process and in the presence of silica vapor (originating from reaction between silicon and oxygen species in the CVD chamber) in the synthesis chamber, these planes provide a suitable surface for SiO_2 formation, thus limiting the growth of Ta_5Si_3 nanocrystals in the $\langle 001 \rangle$ direction. This is clearly shown in TEM observations (Figure 2). A closer look at the crystal structure of the Ta_5Si_3 unit cell (Figure 4) reveals the presence of other planes with a high Si to Ta ratio that can present a suitable surface for SiO_2 formation, further limiting the growth of Ta_5Si_3 in these directions. The deposition rate of silica vapor on these planes is directly related to the silica vapor pressure in the CVD chamber. In the initial region of the CVD chamber, the high concentration of TaCl_5 results in the increase in the partial pressure of silicon species (reaction 1), increasing the silica vapor pressure.

According to the above growth mechanism, high silica vapor pressure enhances the silica coverage of planes parallel to (010) and (001) crystal planes on the nanocrystals, promoting the growth of Ta_5Si_3 networked nanowires shown in Figure 4b. However, with the decrease in concentration of TaCl_5 vapor along the downstream direction of the CVD chamber due to reaction in the initial region (reaction 1), the silica vapor pressure decreases. This decrease enables the partial silica coverage of nanocrystals only on (001) planes (Figure 4c), which reach a critical point during the experiment, causing an imbalance of silica coverage. This results in net mass diffusion of tantalum and silicon species onto {100} planes; thereby, nanoribbons and nanosheets are obtained.

To validate the proposed growth mechanism and reveal the effect of silica vapor pressure on the morphology of Ta_5Si_3 nanostructures, we carried out several experiments by introducing O_2 (increase the silica vapor pressure) and H_2 (decrease the oxygen content and silica vapor pressure) into the system. SEM observations indicated that, with an increase of O_2 content in the CVD chamber, only Ta_5Si_3 NWs were

deposited on the substrate (Figure S1a,b, Supporting Information). However, by introducing the 2% H₂ and Ar, the coverage area of Ta₅Si₃ NNWs and NSs increased (Figure S1c,d, Supporting Information). Further increase of H₂ content resulted in the formation of nano- and microparticles.

Recent publications have reported the superior capacitance performance of silicide nanostructures.⁴ Herein, we have investigated the electrochemical capacitance behavior of the different Ta₅Si₃ nanostructures obtained in this work. Figure 5

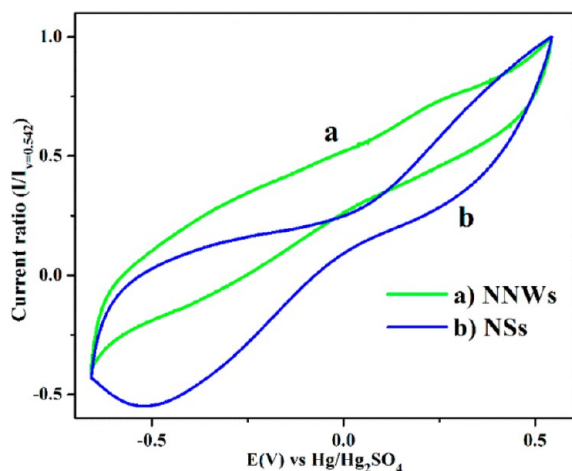


Figure 5. Normalized cyclic voltammograms of the Ta₅Si₃ nanostructures: (a) NNWs and (b) NSs.

shows the normalized cyclic voltammograms of the Ta₅Si₃ NNWs and NSs without any pretreatment. By comparing the area under the curve of line (a) and line (b) in Figure 5, it is apparent that Ta₅Si₃ NSs show a higher capacitance than that of Ta₅Si₃ NNWs. This is in good agreement with previous reports^{31,32} that correspond this increase to the higher surface area of nanosheets compared to networked nanowires. However, because of the presence of the SiO₂ shell layer, it is challenging to calculate the exact capacity of the nanostructures in this stage. Further detailed studies will be needed in our future work.

4. CONCLUSION

We have successfully synthesized single-crystalline Ta₅Si₃ complex nanostructures with a controlled morphology. The nanostructures were deposited on carbon microfibers via LPCVD using tantalum chloride precursor and silicon powder. It was found that the morphology of these nanostructures is very sensitive to precursor and silica partial vapor pressure along the CVD chamber. The networked nanowires are grown in the high Ta concentration region, whereas the networked nanoribbons and nanosheets are grown in the lower Ta concentration area. We proposed a vapor–solid mechanism based on the formation of a silica sheath on {001} crystal planes of Ta₅Si₃ tetragonal nanostructures and their growth evolution with the growth time. Cyclic voltammetry measurements of different morphologies of Ta₅Si₃ nanostructures indicate that networked nanosheets exhibit a superior capacitance compared to other morphologies. The controlled synthesis of single-crystalline 2D Ta₅Si₃ nanostructures as one of the highly stable silicides paves the road for new electronic and energy related applications.

■ ASSOCIATED CONTENT

Supporting Information

Figure S1 shows SEM images of Ta₅Si₃ nanostructures synthesized under the flow of (a, b) O₂ and Ar and (c, d) 2% (flow rate) H₂ and Ar. This material is available free of charge via the Internet at <http://pubs.acs.org>.

■ AUTHOR INFORMATION

Corresponding Author

*Phone: 1-519-661-2111, ext. 87759. Fax: 1-519-661-3020. E-mail: xsun@eng.uwo.ca. <http://www.eng.uwo.ca/people/asun/default.htm>.

Notes

The authors declare no competing financial interest.

■ ACKNOWLEDGMENTS

This research was supported by General Motors of Canada, the Natural Sciences and Engineering Research Council of Canada, Ontario Centers of Excellence, Canada Research Chair Program, the Canada Foundation for Innovation, and the University of Western Ontario.

■ REFERENCES

- (1) Cui, C.; Zhang, J.; Liu, L.; Fu, H. *J. Mater. Sci. Technol.* **2010**, *26*, 65–68.
- (2) Schmitt, A. L.; Higgins, J. M.; Szczech, J. R.; Jin, S. *J. Mater. Chem.* **2010**, *20*, 223–235.
- (3) Chou, L.-J.; Chueh, Y.-L.; Ko, M.-T. *Thin Solid Films* **2007**, *515*, 8109–8112.
- (4) Zhang, Y.; Geng, D.; Liu, H.; Banis, M. N.; Ionescu, M. I.; Li, R.; Cai, M.; Sun, X. *J. Phys. Chem. C* **2011**, *115*, 15885–15889.
- (5) Chueh, Y. L.; Chou, L. J.; Cheng, S. L.; Chen, L. J.; Tsai, C. J.; Hsu, C. M.; Kung, S. C. *Appl. Phys. Lett.* **2005**, *87*, 223113.
- (6) Reader, A. H.; van Ommen, A. H.; Weijss, P. J. W.; Wolters, R. A. M.; Oostra, D. J. *Rep. Prog. Phys.* **1993**, *56*, 1397–1467.
- (7) Chirkin, A. D.; Lavrenko, V. O.; Talash, V. M. *Powder Metall. Met. Ceram.* **2009**, *48*, 330–345.
- (8) Gong, Q.-M.; Li, Z.; Wang, Y.; Wu, B.; Zhang, Z.; Liang, J. *Mater. Res. Bull.* **2007**, *42*, 474–481.
- (9) Cheb, J. L. *JOM* **2005**, *57*, 24–30.
- (10) Borghesi, A.; Nosenzo, L.; Piaggi, A.; Guizzetti, G.; Nobili, C.; Ottaviani, G. *Phys. Rev. B: Condens. Matter Mater. Phys.* **1988**, *38*, 10937–10940.
- (11) Amiotti, M.; Borghesi, A.; Marabelli, F.; Piaggi, A.; Guizzetti, G.; Nava, F. *Appl. Surf. Sci.* **1991**, *53*, 230–236.
- (12) Chueh, Y.-L.; Ko, M.-T.; Chou, L.-J.; Chen, L.-J.; Wu, C.-S.; Chen, C.-D. *Nano Lett.* **2006**, *6*, 1637–1644.
- (13) Zhang, S.-L.; Ostling, M. *Crit. Rev. Solid State Mater. Sci.* **2003**, *28*, 1–129.
- (14) Maszara, W. P. *J. Electrochem. Soc.* **2005**, *152*, G550–G555.
- (15) Viennois, R.; Tao, X.; Jund, P.; Tedenac, J.-C. *J. Electron. Mater.* **2011**, *40*, 597–600.
- (16) Chen, L. J.; Wu, W.-W.; Hsu, H. C.; Chen, S. Y.; Chueh, Y. L.; Chou, L.-J.; Lu, K. C.; Tu, K. N. *ECS Trans.* **2007**, *11*, 3–6.
- (17) Zhou, S.; Liu, X.; Lin, Y.; Wang, D. *Chem. Mater.* **2009**, *21*, 1023–1027.
- (18) Kim, T.; Bird, J. P. *Appl. Phys. Lett.* **2010**, *97*, 263111.
- (19) Zhang, H.-L. *Nanotechnology* **2008**, *19*, 1–7.
- (20) Saha, M. S.; Banis, M. N.; Zhang, Y.; Li, R.; Sun, X.; Cai, M.; Wagner, F. T. *J. Power Sources* **2009**, *192*, 330–335.
- (21) Saha, M. S.; Li, R.; Cai, M.; Sun, X. *Electrochem. Solid-State Lett.* **2007**, *10*, B130–B133.
- (22) Rao, C. N.; Deepak, F.; Gundiah, G.; Govindaraj, A. *Prog. Solid State Chem.* **2003**, *31*, 5–147.
- (23) Williams, D. S.; Coleman, E.; Brown, J. M. *J. Electrochem. Soc.* **1986**, *133*, 2637–2644.

- (24) Widmer, A. E.; Fehlmann, R. *Thin Solid Films* **1986**, *138*, 131–140.
- (25) Zhou, S. *Angew. Chem., Int. Ed.* **2008**, *47*, 7681–7684.
- (26) Banis, M. N.; Zhang, Y.; Banis, H. N.; Li, R.; Sun, X.; Jiang, X.; Nikanpour, D. *Chem. Phys. Lett.* **2011**, *501*, 470–474.
- (27) Zhang, H.-X.; Ge, J.-P.; Wang, J.; Li, Y.-D. *Nanotechnology* **2006**, *17*, S253–S261.
- (28) Ye, C.; Fang, X.; Hao, Y.; Teng, X.; Zhang, L. *J. Phys. Chem. B* **2005**, *109*, 19758–19765.
- (29) Zhang, H.-X.; Ge, J.-P.; Li, Y.-D. *J. Phys. Chem. B* **2006**, *110*, 14107–14113.
- (30) Zhang, Y.; Li, R.; Zhou, X.; Cai, M.; Sun, X. *J. Nanomater.* **2008**, *2008*, 1–8.
- (31) Yang, S.-Y.; Chang, K.-H.; Tien, H.-W.; Lee, Y.-F.; Li, S.-M.; Wang, Y.-S.; Wang, J.-Y.; Ma, C.-C. M.; Hu, C.-C. *J. Mater. Chem.* **2011**, *21*, 2374–2380.
- (32) Xiong, S.; Yuan, C.; Zhang, X.; Xi, B.; Qian, Y. *Chem.—Eur. J.* **2009**, *15*, 5320–5326.